Supporting Information

Making the Inverted Keggin Ion Lacunary

Lu-Lu Liu,[a] Zi-Yu Xu,[a] Peng Yi,[a] Chao-Qin Chen,[a] Zhong-Ling Lang,[b]* and Peng Yang[a]*

a College of Chemistry and Chemical Engineering
Advanced Catalytic Engineering Research Center of the Ministry of Education
Hunan University, Changsha 410082, P. R. China

b Key Laboratory of Polyoxometalate and Reticular Material Chemistry of Ministry of Education
Faculty of Chemistry
Northeast Normal University, Changchun 130024, P. R. China

Corresponding Author

*E-mail: pengyang216@hnu.edu.cn (P.Y.)

*E-mail: langzl554@nenu.edu.cn (Z.-L.L.)

Table of Contents (31 pages)

1. Experimental Details

1.1 Materials

Unless otherwise indicated, all chemicals and reagents were purchased from commercial suppliers and used without further purification.

1.2 Physical measurements

FT-IR. The Fourier transform infrared (FT-IR) spectra were recorded on KBr disk using a Shimadzu IRSpirit-T spectrometer between 400 and 4000 cm^{-1}.

Elemental Analyses. CHN microanalyses were performed on a Perkin-Elmer 240C elemental analyzer, and ICP-OES analyses were performed on a Perkin-Elmer Optima 8300 optical emission spectrometer.

NMR. The ^{1}H and ^{13}C nuclear magnetic resonance (NMR) spectra were recorded on a Bruker Avance III 400 MHz instrument at room temperature, using 5-mm tubes for ^{1}H and ^{13}C with respective resonance frequencies of 399.78 MHz (^{1}H) and 100.71 MHz (^{13}C).

TGA. Thermogravimetric analyses (TGA) were carried out on a TA Instruments SDT Q600 thermobalance with a 100 mL min^{-1} flow of nitrogen; the temperature was ramped from 25 to 800 °C at a rate of 5 °C min^{-1}.

ESI-MS. The electrospray-ionization mass spectrometry (ESI-MS) measurements were made in the negative ion mode on an Agilent 6520 Q-TOF LC/MS mass spectrometer coupled to an Agilent 1200 LC system, and all the MS data were processed by the MassHunter Workstation software. Sample solutions were ca. 10^{-5} M in water and were transferred to the electrospray source by direct injection.

Powder XRD. Powder X-ray diffraction (Powder XRD) patterns were obtained using a Bruker D8 ADVANCE diffractometer with Cu *Ka* radiation (λ = 1.54056 Å).

XPS. For X-ray photoelectron spectroscopy (XPS), a 100-nm-thick Ag film was deposited by sputter-coating on a silicon substrate. The samples were then dispersed in acetone and drop-casted on the Ag coated silicon substrate. After sample preparation, they were introduced into the XPS vacuum chamber equipped with a photoelectron spectrometer consisting of a hemispherical analyzer (Spec Phoebos 100) and a Mg/Al X-ray source (Spec XR-50). For excitation, the Mg Kα (E = 1253.6 eV) anode was used. The shift in the binding energy due to surface charging was corrected with respect to the C 1s peak. The data evaluation was done by CASAXPS software.

EDX. Energy dispersive X-Ray (EDX) spectra were acquired on a JEM-2100Plus instrument.

UV-vis Absorption. The ultraviolet-visible (UV-vis) absorption spectra were measured at room temperature using a Shimadzu UV-1900i spectrophotometer.

SEM. Scanning electron microscopy (SEM) images were acquired on a Hitachi Regulus 8100 instrument.

Nitrogen Adsorption-Desorption Isotherm. Nitrogen physisorption isotherms were measured at 77 K using BSD-660M A6B6M apparatus to determine the Brunauer−Emmett−Teller (BET) surface area.

The samples were pre-degassed at 343 K under vacuum for 14 h.

X-ray Crystallography. Single crystals of the three compounds were mounted in a Hampton cryoloop with light oil to prevent efflorescence. The data collections for these compounds were performed at 150 K on a Bruker D8 Quest single-crystal diffractometer equipped with Mo *K*α radiation (λ = 0.71073 Å). All structures were solved with the ShelXT structure solution program using Intrinsic Phasing[S1] and refined with the ShelXL refinement package using Least Squares minimization[S2] operated in the OLEX2 interface.[S3] All non-hydrogen atoms were refined anisotropically. The hydrogen atoms of the organic groups were introduced in geometrically calculated positions. It was not possible to locate all counter cations by X-ray diffraction, probably due to crystallographic disorder, which is a common problem in polyoxometalate crystallography. Thus, the SQUEEZE program[S4] or the Olex2 solvent mask function were further used to remove the contributions of weak reflections from the whole data. The newly generated hkl data were further used to refine the final crystal data. Therefore, the exact number of cations and solvent molecules was determined by elemental analysis and thermogravimetric diagrams. The resulting formula units were further used throughout the paper. In the Supporting Information, the crystal data and structure refinement for the three compounds is summarized in Table S7. CCDC-2367552 (**$SeAs_3Mo_{10}$**), CCDC-2367554 (**$Se_2As_2Mo_{10}$**), and CCDC- 2367553 (**$Se_2As_6Mo_{20}Ce_2$**) contain the supplementary crystallographic data for this paper. These data can be obtained free of charge from The Cambridge Crystallographic Data Center via www.ccdc.cam.ac.uk/data_request/cif.

Basic Procedure of the Condensation-Cyclization Reaction. Hydrazine (0.2 mmol), 1,3-diketone (0.2 mmol), catalyst (1.5 mol%), and DMC (dimethyl carbonate, 0.5 mL) were added to a 5-mL reaction vial with a Teflon screw cap. Then the reaction was carried out at varying temperature and time. After the reaction was complete, the mixture was purified by column chromatography on silica gel (200-300 mesh) using petroleum ether (60-90 °C) and ethyl acetate to obtain the desired products.

Basic Procedure of the Acetalization Reaction. 2-aminobenzamide (0.2 mmol), benzaldehyde (0.2 mmol), catalyst (1.5 mol%), and acetonitrile (1.0 mL) were added to a 5-mL reaction vial with a Teflon screw cap. Then the reaction was carried out at 80 °C and different reaction time. After the reaction was complete, the mixture was purified by column chromatography on silica gel (200-300 mesh) using petroleum ether (60-90 °C) and ethyl acetate to obtain the desired products.

DFT computational details: To qualitatively compare the surface electronic character between the plenary **As_4Mo_{12}** as well as lacunary **$SeAs_3Mo_{10}$** and **$Se_2As_2Mo_{10}$** molecules, the electrostatic potential distribution was computed for the three polyanions with density functional theory method. All calculations were performed through the facilities provided by the Gaussian09 package.[S5] Geometry optimizations were carried out with B3LYP functional, and the LANL2DZ basis set was employed for the Mo atom, whereas the 6–31G (d, p) basis set was used for the H, C, N, Se, As, and O atoms.[S6] The continuum PCM implicit solvation model was used to simulate the effect of the aqueous solution.[S7]

2. Synthesis of Compounds

Synthesis of $(NH_4)_3[(SeO_3)(p\text{-}H_3NC_6H_4AsO_3)_3Mo_{10}O_{29}]\cdot 15H_2O$ ($SeAs_3Mo_{10}$)

$(NH_4)_6Mo_7O_{24}\cdot 4H_2O$ (2.001 g, 1.619 mmol), SeO_2 (0.201 g, 1.811 mmol), *p*-aminophenylarsonic acid (0.199 g, 0.917 mmol), and glycine (0.200 g, 5.328 mmol) were dissolved in 15 mL of distilled water for 20 min upon stirring. Then, the pH of the above solution was adjusted to 0.9 using HCl (6 M). The mixture was stirred and heated at 90 °C for 2 h, cooled to room temperature and filtered. Slow evaporation of the filtrate in an open vial resulted in block-shaped, dark yellow crystals after two weeks, which were then collected by filtration and air dried. Yield: 0.255 g (33% based on *p*-aminophenylarsonic acid). Elemental analysis (%): Calcd: C 8.57, N 3.33, Se 3.13, As 8.91, Mo 38.03; Found: C 8.14, N 3.51, Se 3.28, As 8.44, Mo 38.56. IR (2% KBr pellet, ν/cm^{-1}): 3426 (w), 1632 (m), 1419 (m), 1396 (m), 1096 (s), 913 (s), 855 (s), 670 (s), 549 (s).

Synthesis of $(NH_4)_4[(SeO_3)_2(p\text{-}H_3NC_6H_4AsO_3)_2Mo_{10}O_{29}]\cdot 11H_2O$ ($Se_2As_2Mo_{10}$)

$(NH_4)_6Mo_7O_{24}\cdot 4H_2O$ (2.001 g, 1.619 mmol), SeO_2 (0.300 g, 2.750 mmol), and *p*-aminophenylarsonic acid (0.199 g, 0.917 mmol) were dissolved in 15 mL of distilled water for 20 min upon stirring. Then, the pH was adjusted to 1.1 using HCl (6 M). The mixture was stirred and heated at 90 °C for 30 min, cooled to room temperature and filtered. Slow evaporation of the filtrate in an open vial resulted in rod-shaped, colorless crystals after one week, which were then collected by filtration and air dried. Yield: 0.305 g (28% based on *p*-aminophenylarsonic acid). Elemental analysis (%): Calcd: C 6.06, N 3.53, Se 6.64, As 6.30, Mo 40.32; Found: C 5.73, N 3.23, Se 6.36, As 6.44, Mo 39.56. IR (2% KBr pellet, ν/cm^{-1}): 3430 (w), 3150 (w), 1732 (m), 1625 (m), 1504 (m), 1405 (m), 1133 (m), 1073 (m), 914 (s), 853 (s), 650 (s), 569 (s).

Synthesis of $[\{Ce(H_2O)_6(SeO_3)(p\text{-}H_3NC_6H_4AsO_3)_3Mo_{10}O_{29}\}_2]\cdot 35H_2O$ ($Se_2As_6Mo_{20}Ce_2$)

Precursor Approach: $SeAs_3Mo_{10}$ (0.252 g, 0.100 mmol) and $Ce(NO_3)_3\cdot 6H_2O$ (0.201 g, 0.463 mmol) were dissolved in 15 mL of distilled water for 20 min upon stirring. Then, the pH of the above solution was adjusted to 1.2 using HCl (6 M). The mixture was stirred and heated at 90 °C for 2 h, cooled to room temperature and filtered. Slow evaporation of the filtrate in an open vial resulted in block-shaped, yellow crystals after two weeks, which were then collected by filtration and air dried. Yield: 0.083 g (15% based on **$SeAs_3Mo_{10}$**). Elemental analysis (%): Calcd: C 7.83, N 1.52, Se 2.86, As 8.14, Ce, 5.07, Mo 34.74; Found: C 8.02, N 1.78, Se 2.69, As 8.24, Ce, 4.47, Mo 35.32. IR (2% KBr pellet, ν/cm^{-1}): 3438 (w), 3134 (w), 2808 (w), 1629 (m), 1544 (m), 1414 (m), 946 (s), 876 (s), 702 (s), 668 (s).

In situ Approach: $(NH_4)_6Mo_7O_{24}\cdot 4H_2O$ (2.001 g, 1.619 mmol), SeO_2 (0.201 g, 1.811 mmol), *p*-aminophenylarsonic acid (0.199 g, 0.917 mmol), and $Ce(NO_3)_3\cdot 6H_2O$ (0.300 g, 0.691 mmol) were dissolved in 15 mL of distilled water for 20 min upon stirring. Then, the pH of the above solution was adjusted to 1.2 using HCl (6 M). The mixture was stirred and heated at 90 °C for 2 h, cooled to room temperature and filtered. Slow evaporation of the filtrate in an open vial resulted in block-shaped, yellow crystals after two weeks, which were then collected by filtration and air dried. Yield: 0.405 g (24% based on *p*-aminophenylarsonic acid).

3. Characterizations on Compounds

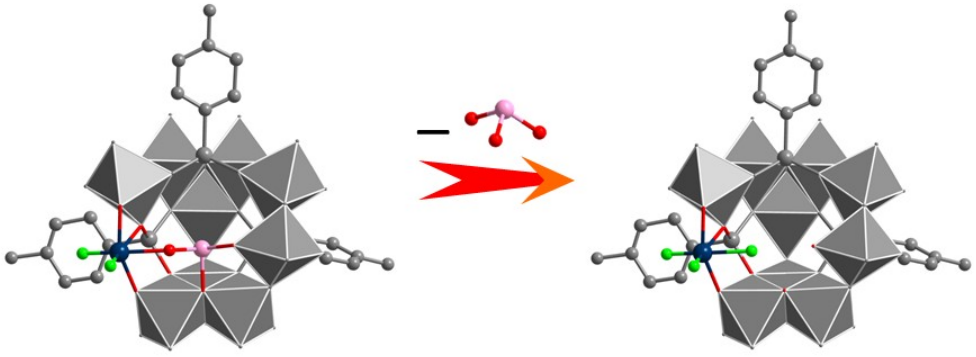

Fig. S1. Structural representation of the expected three terminal metal–oxygen bonds in a *mer* fashion. The terminal oxygen atoms are marked in green color.

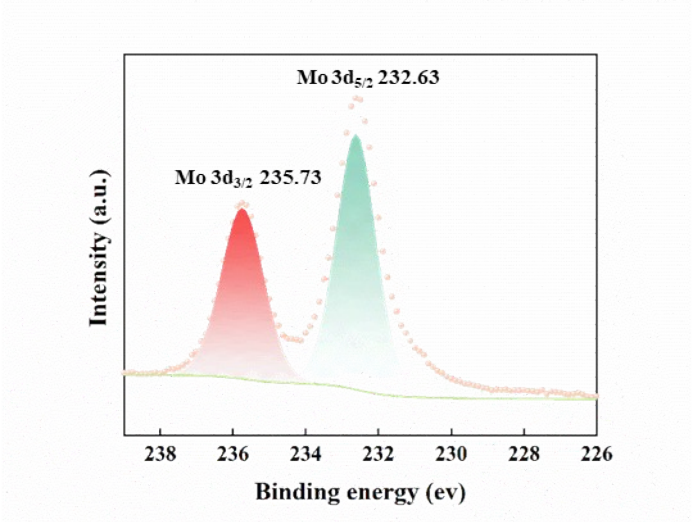

Fig. S2. XPS analysis for Mo^{VI} in **$SeAs_3Mo_{10}$**.

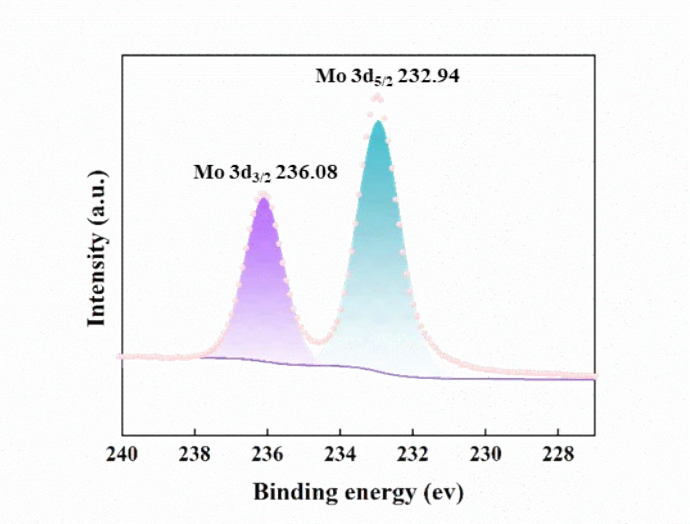

Fig. S3. XPS analysis for Mo^{VI} in **$Se_2As_2Mo_{10}$**.

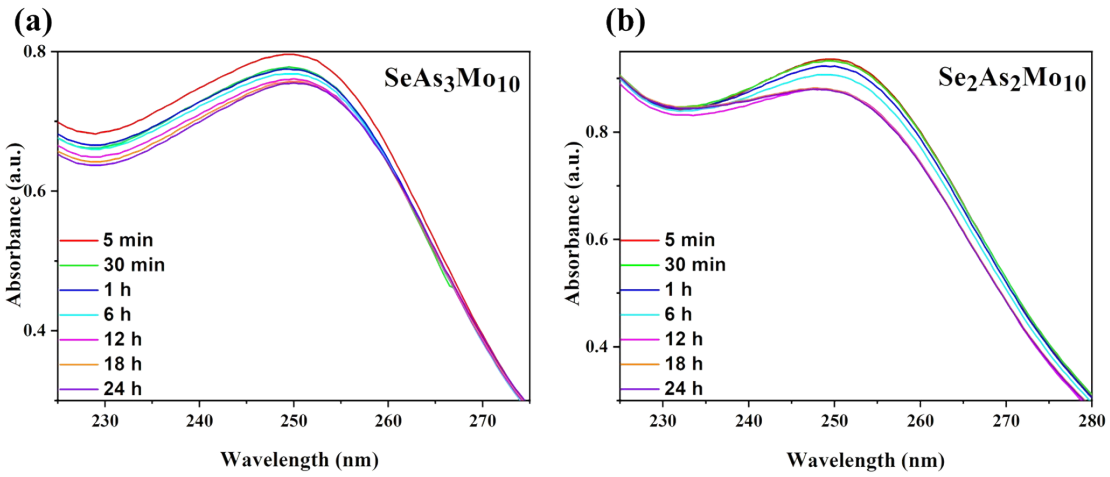

Fig. S4. UV-vis spectra of the aqueous solution containing **$SeAs_3Mo_{10}$** (a) and **$Se_2As_2Mo_{10}$** (b) at different time intervals.

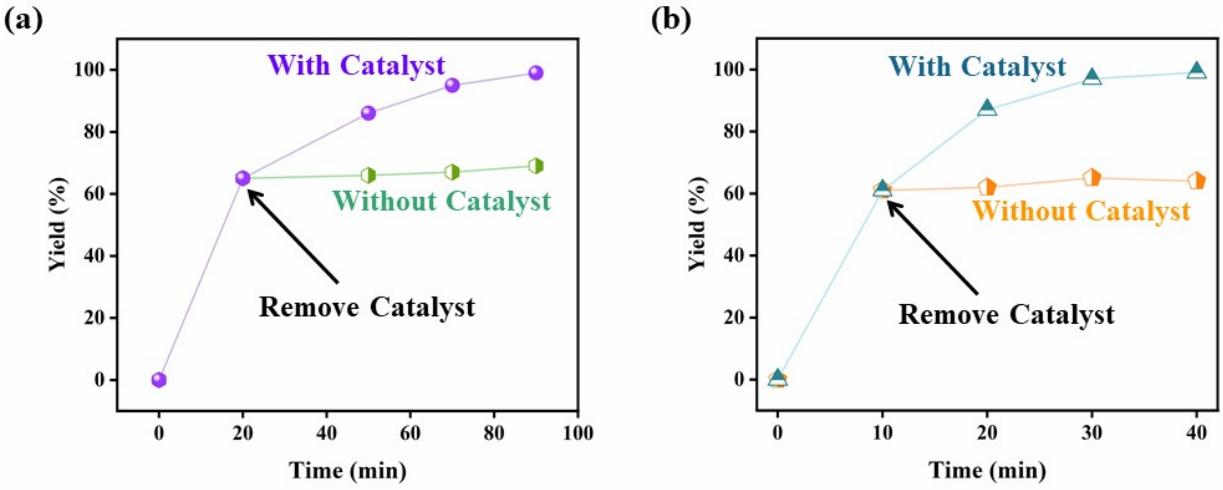

Fig. S5. (a) The filtration test of $SeAs_3Mo_{10}$ as heterogeneous catalyst. (b) The filtration test of $Se_2As_6Mo_{20}Ce_2$ as heterogeneous catalyst.

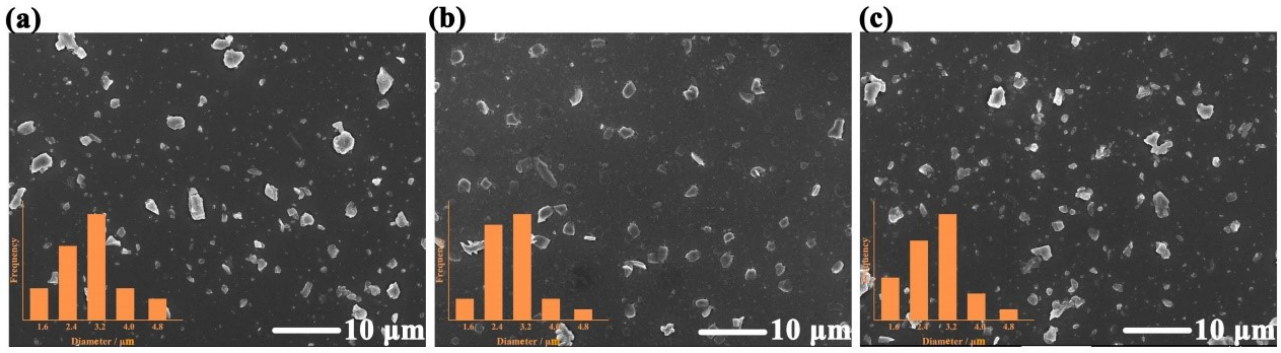

Fig. S6. SEM images and average size distribution of $SeAs_3Mo_{10}$ (a), $Se_2As_2Mo_{10}$ (b), and $Se_2As_6Mo_{20}Ce_2$ (c).

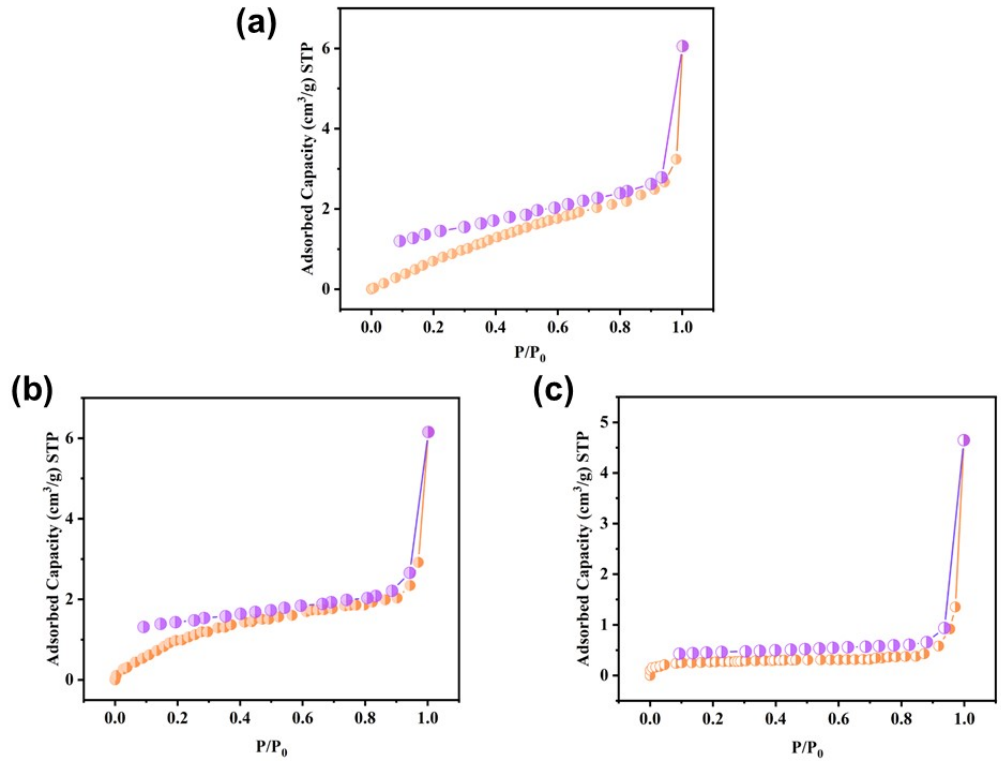

Fig. S7. N_2 adsorption (orange) and desorption (purple) curves of **$SeAs_3Mo_{10}$** (a), **$Se_2As_2Mo_{10}$** (b), and **$Se_2As_6Mo_{20}Ce_2$** (c) at 77 K.

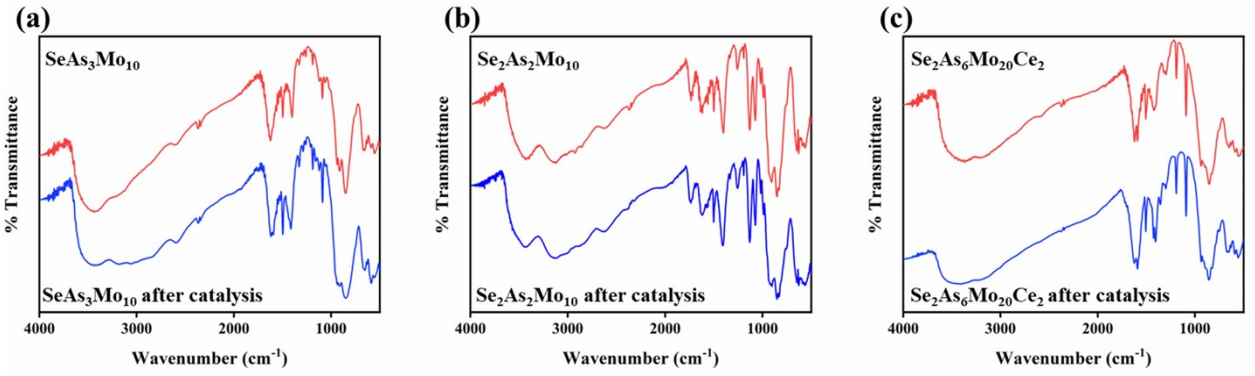

Fig. S8. FT-IR spectra of **$SeAs_3Mo_{10}$** (a), **$Se_2As_2Mo_{10}$** (b) and **$Se_2As_6Mo_{20}Ce_2$** (c) before and after catalysis.

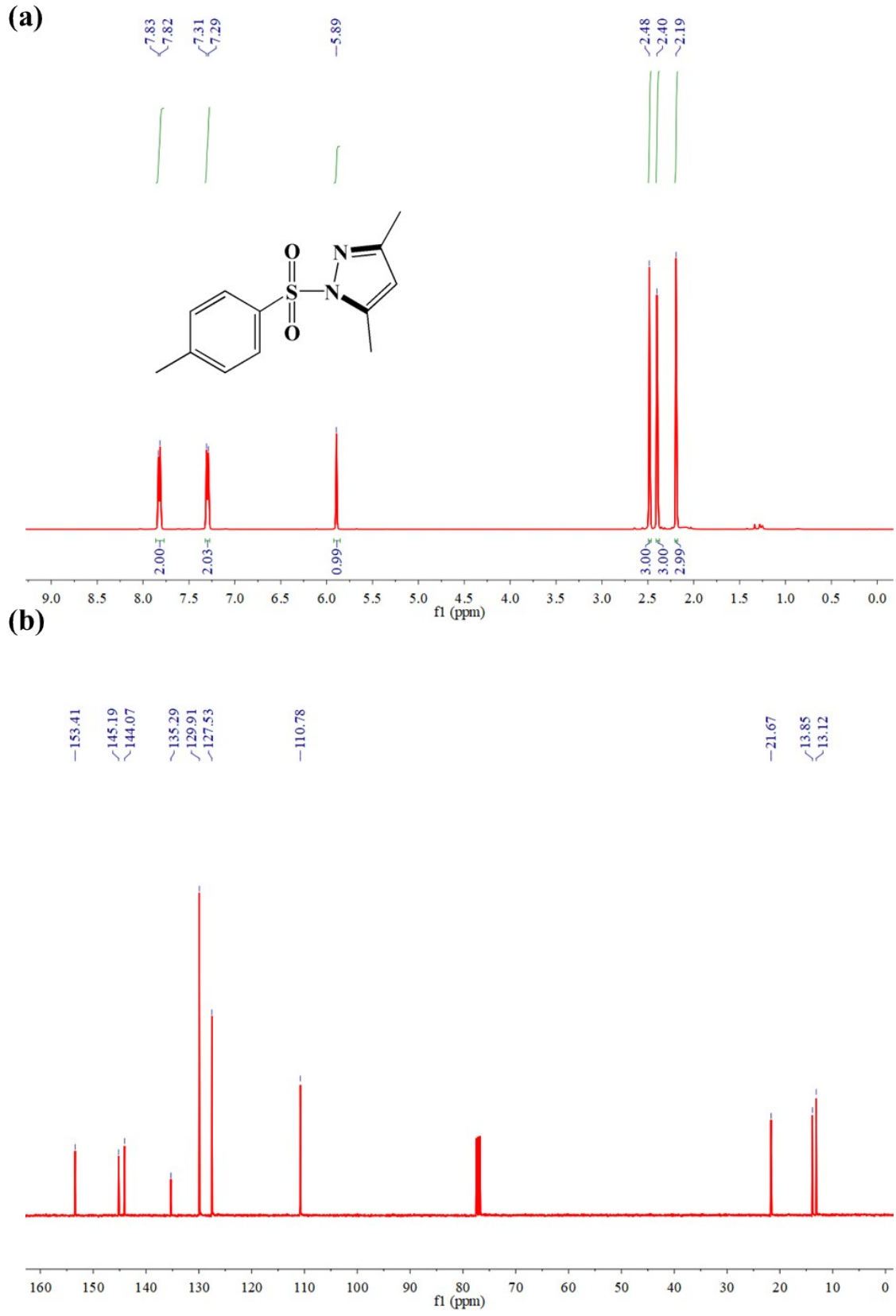

Fig. S9. ^{1}H NMR (a) and ^{13}C NMR (b) spectra of 3,5-dimethyl-1-tosyl-1H-pyrazole (**3a**).

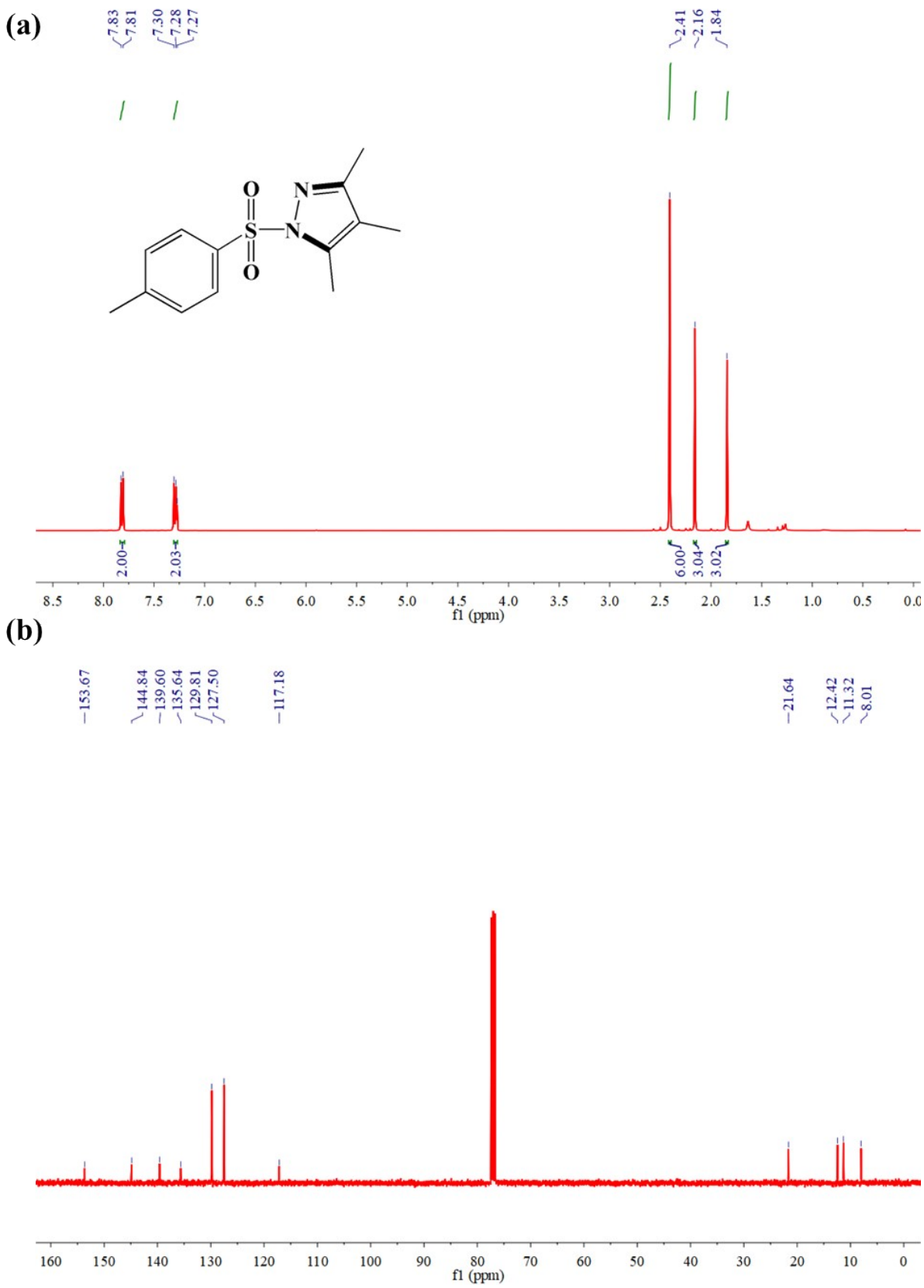

Fig. S10. ^{1}H NMR (a) and ^{13}C NMR (b) spectra of 3,4,5-trimethyl-1-tosyl-1H-pyrazole (**3b**).

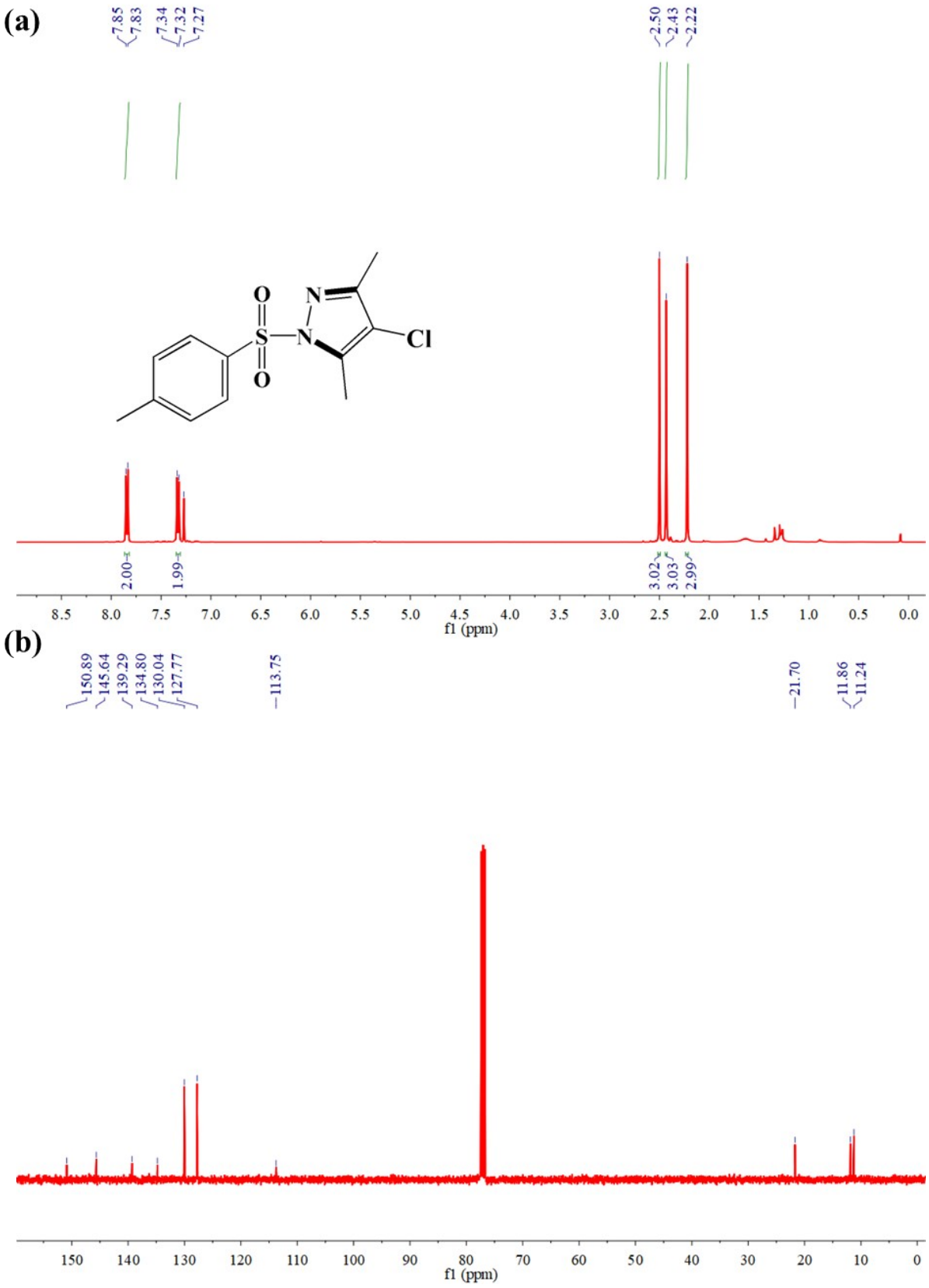

Fig. S11. ^{1}H NMR (a) and ^{13}C NMR (b) spectra of 4-chloro-3,5-dimethyl-1-tosyl-1H-pyrazole (**3c**).

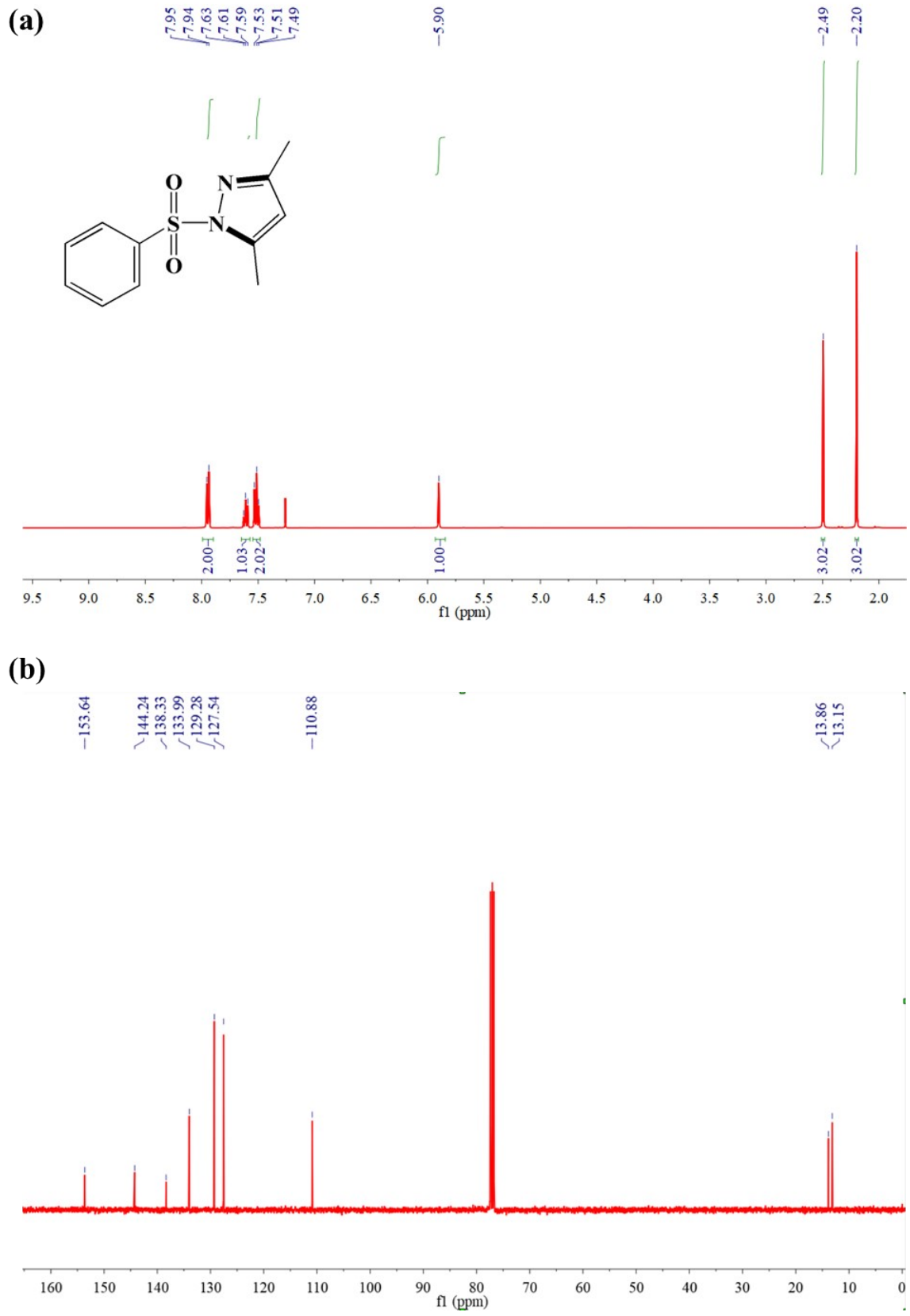

Fig. S12. ^{1}H NMR (a) and ^{13}C NMR (b) spectra of 3,5-dimethyl-1-(phenylsulfonyl)-1H-pyrazole (**3d**).

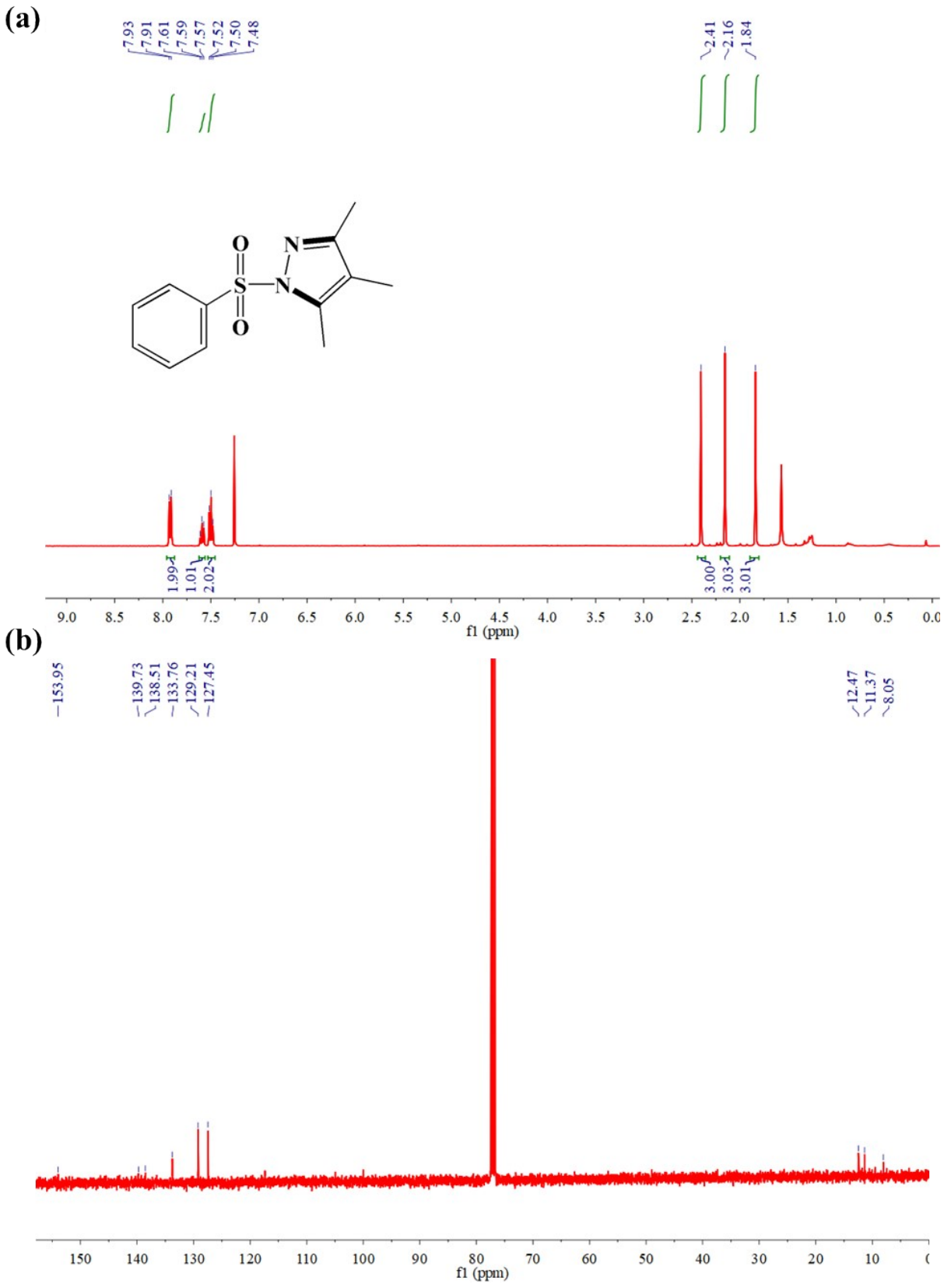

Fig. S13. ^{1}H NMR (a) and ^{13}C NMR (b) spectra of 3,4,5-trimethyl-1-(phenylsulfonyl)-1H-pyrazole (**3e**).

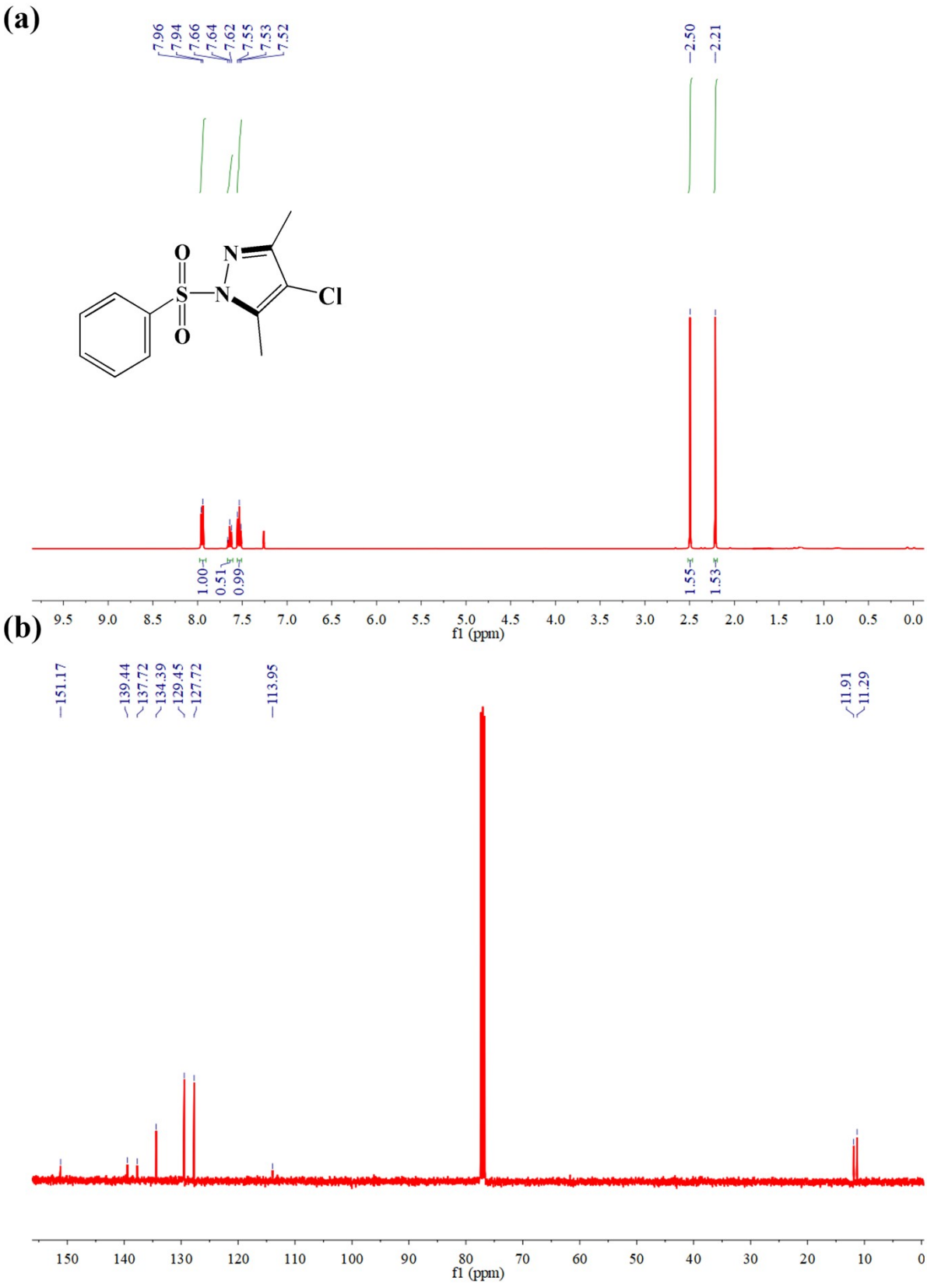

Fig. S14. ^{1}H NMR (a) and ^{13}C NMR (b) spectra of 4-chloro-3,5-dimethyl-1-(phenylsulfonyl)-1H-pyrazole (**3f**).

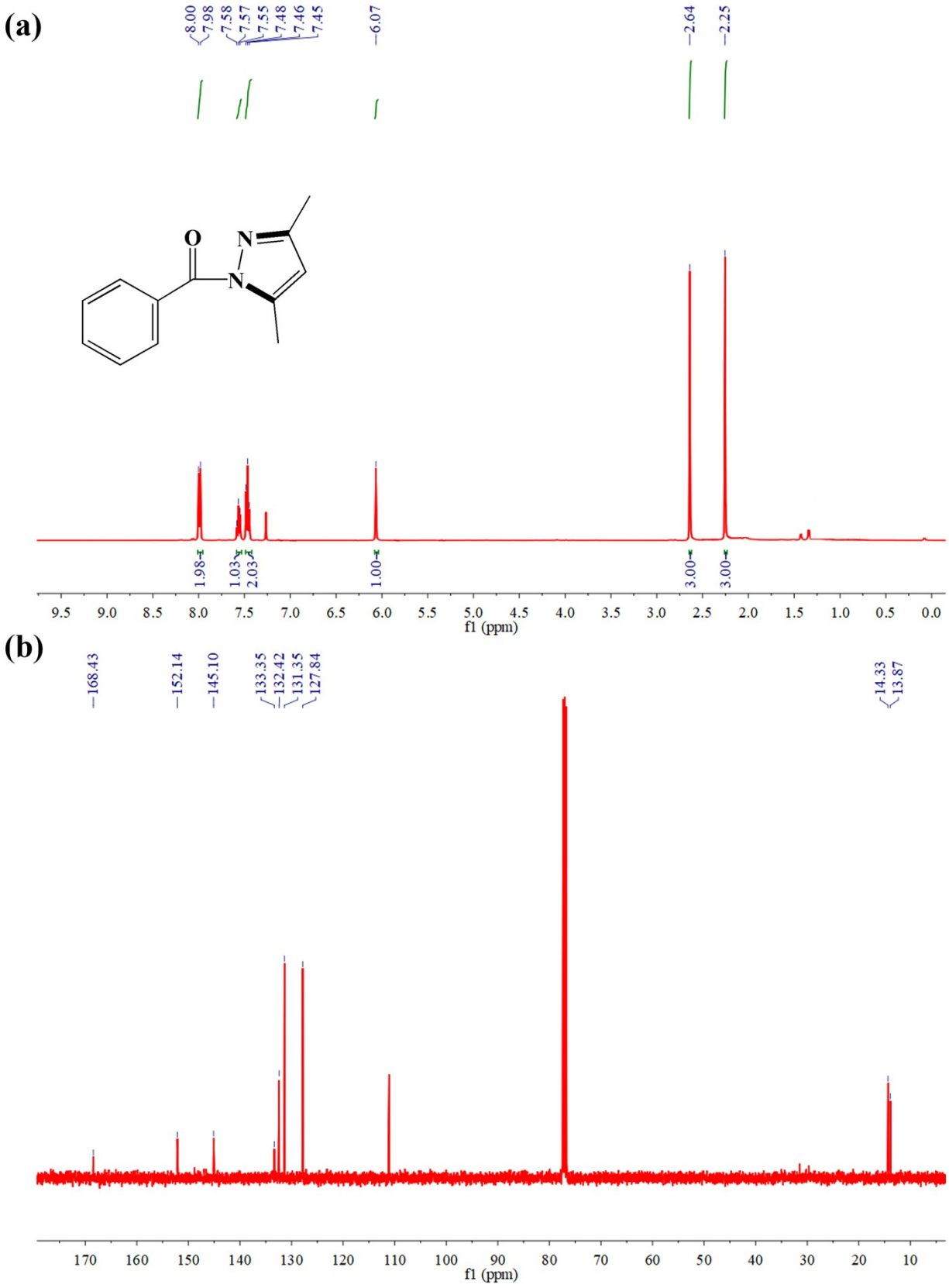

Fig. S15. ^{1}H NMR (a) and ^{13}C NMR (b) spectra of (3,5-dimethyl-1*H*-pyrazol-1-yl)(phenyl)methanone (**3g**).

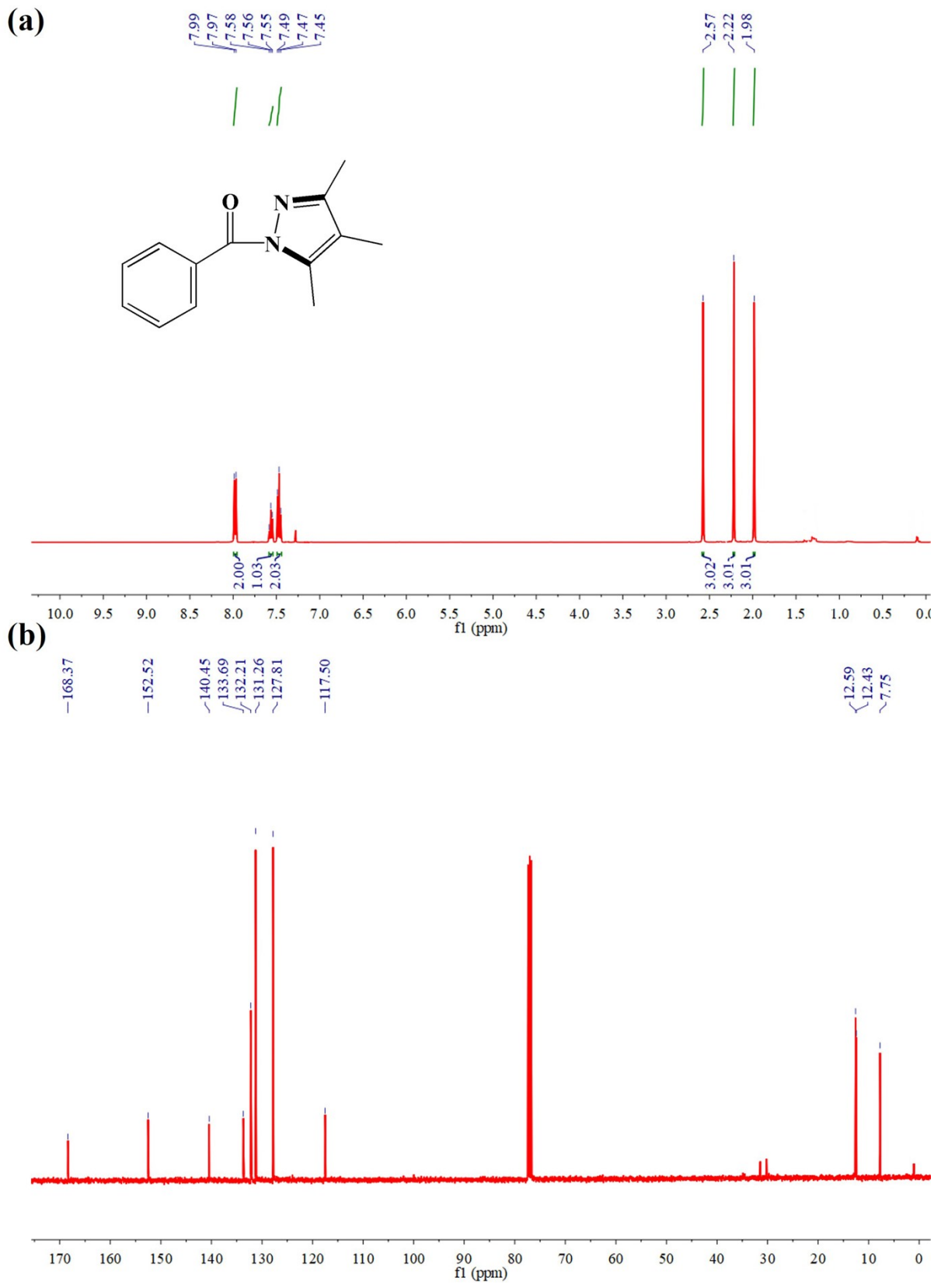

Fig. S16. ^{1}H NMR (a) and ^{13}C NMR (b) spectra of phenyl(3,4,5-trimethyl-1H-pyrazol-1-yl) methanone (**3h**).

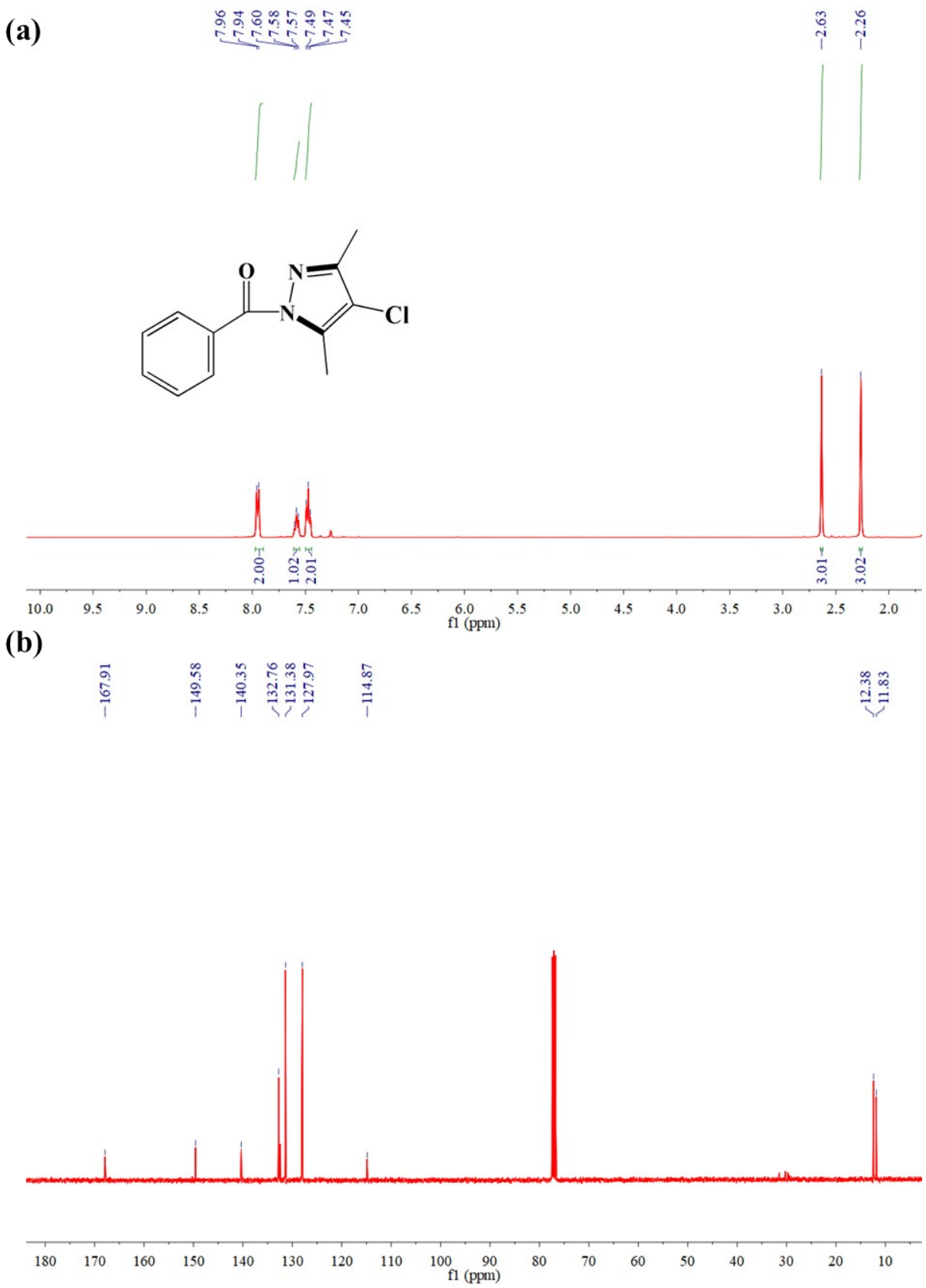

Fig. S17. ^{1}H NMR (a) and ^{13}C NMR (b) spectra of (4-chloro-3,5-dimethyl-1H-pyrazol-1-yl)(phenyl)methanone (**3i**).

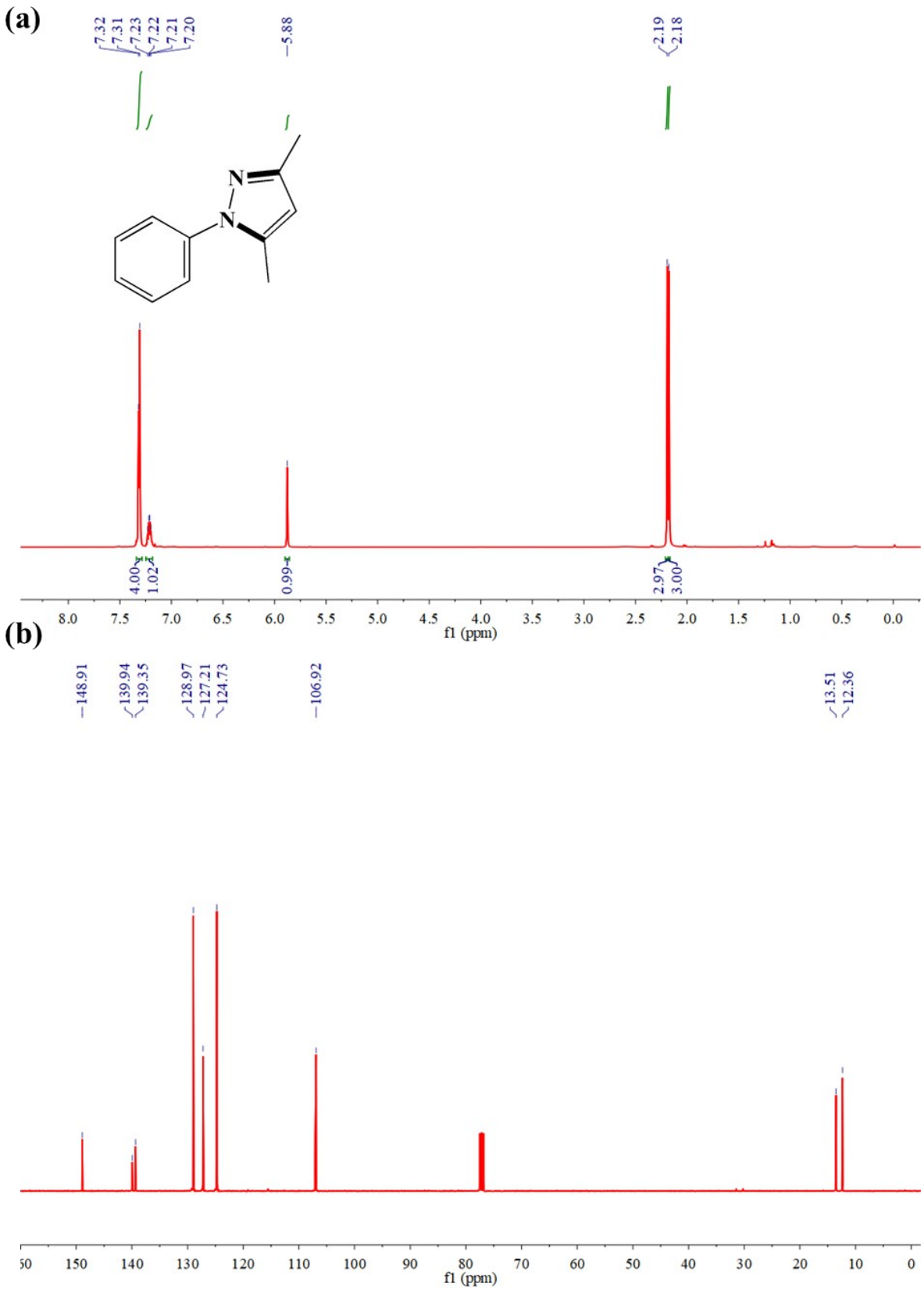

Fig. S18. ^{1}H NMR (a) and ^{13}C NMR (b) spectra of 3,5-dimethyl-1-phenyl-1H-pyrazole (**3j**).

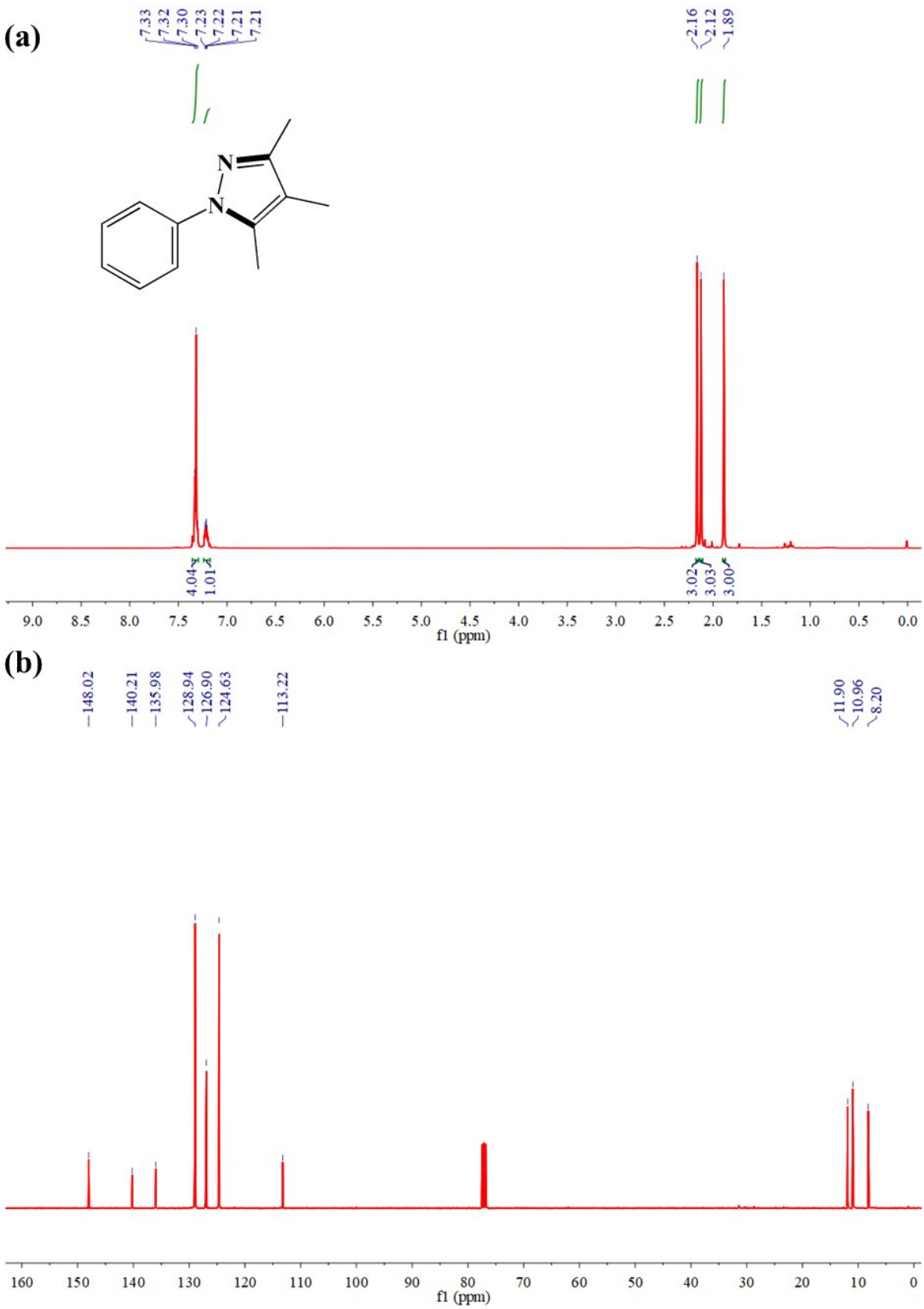

Fig. S19. ^{1}H NMR (a) and ^{13}C NMR (b) spectra of 3,4,5-trimethyl-1-phenyl-1H-pyrazole (**3k**).

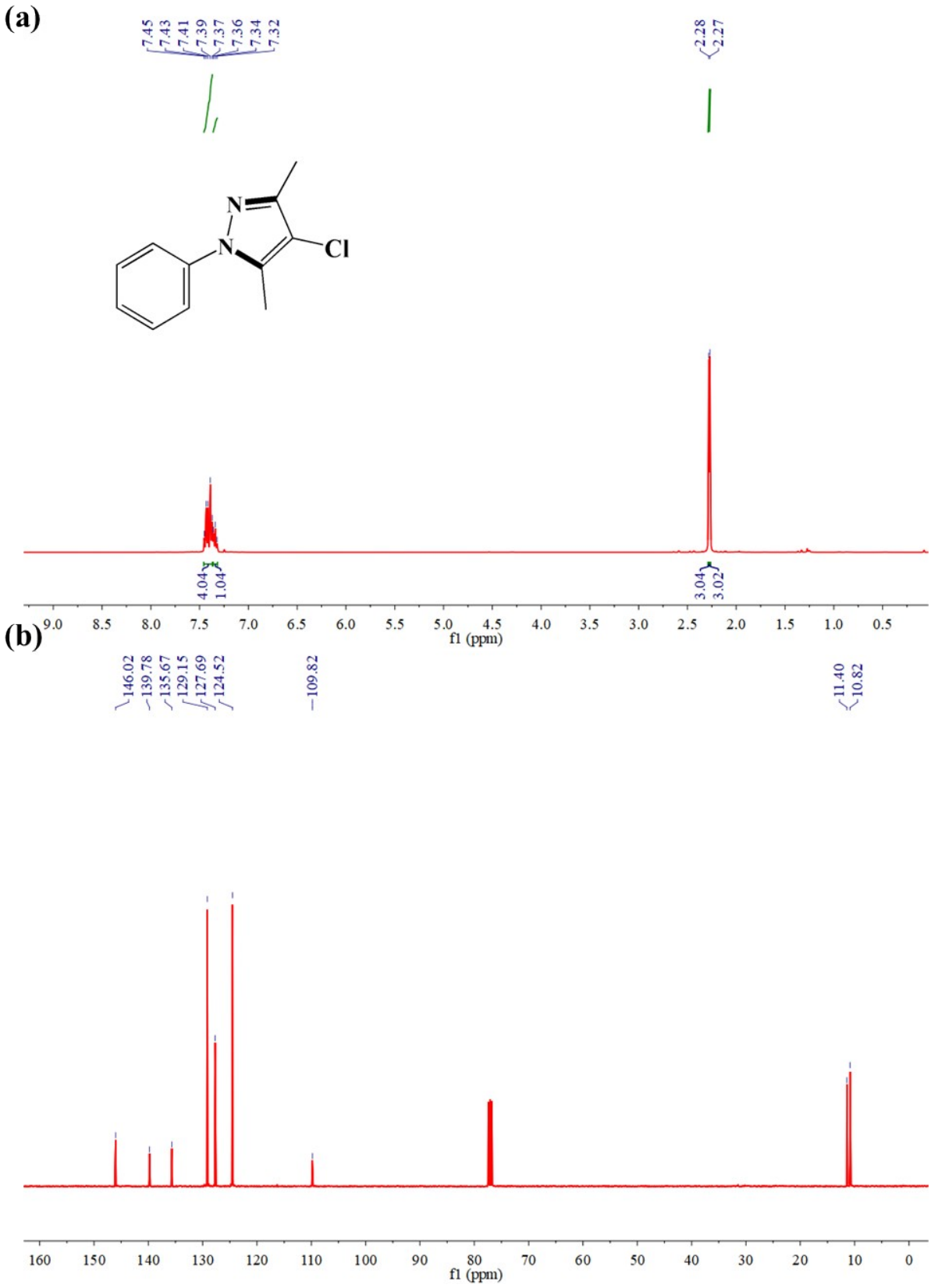

Fig. S20. ^{1}H NMR (a) and ^{13}C NMR (b) spectra of 4-chloro-3,5-dimethyl-1-phenyl-1H-pyrazole (**3l**).

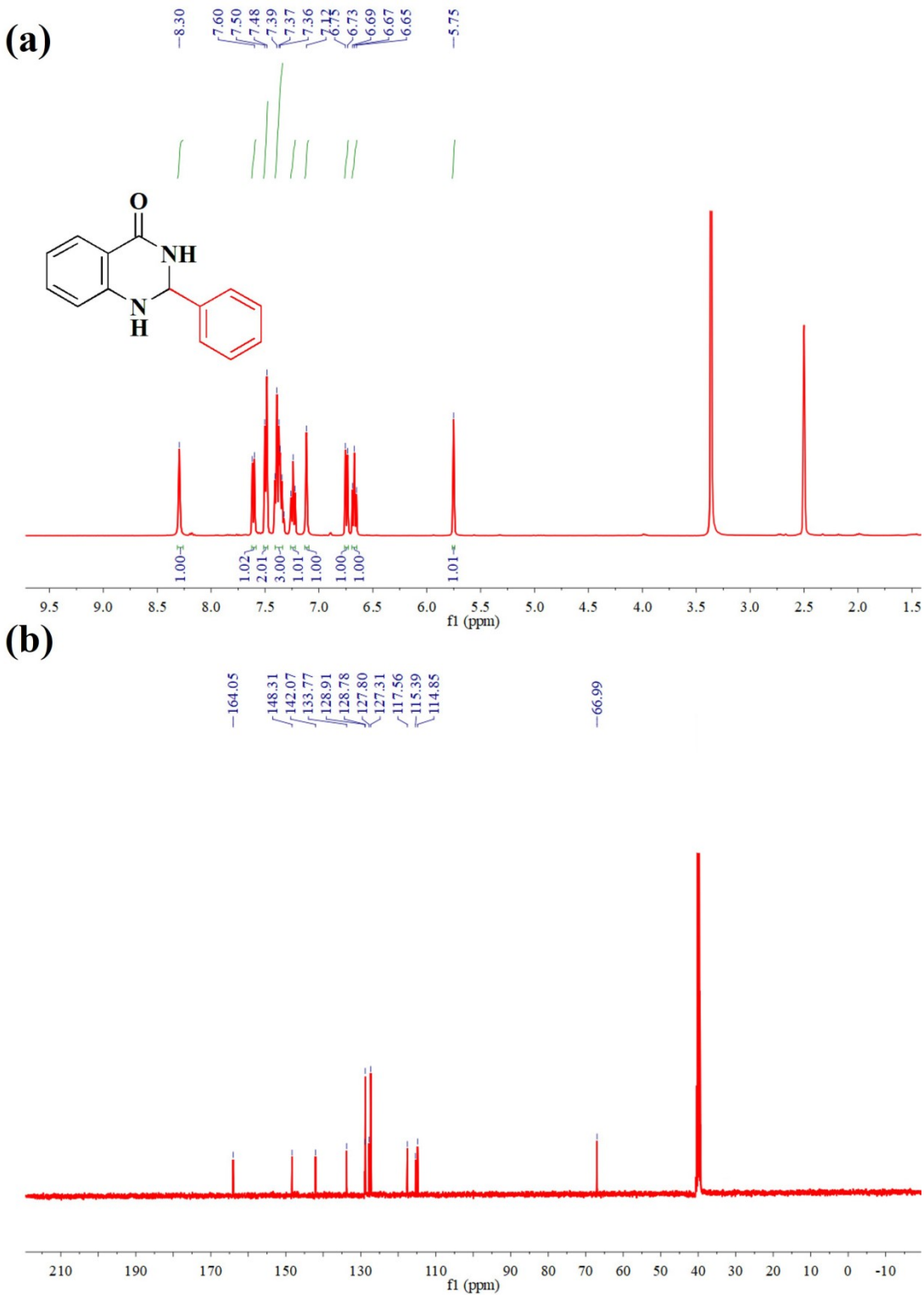

Fig. S21. ^{1}H NMR (a) and ^{13}C NMR (b) spectra of 2-Phenyl-2,3-dihydroquinazolin-4(1H)-one.

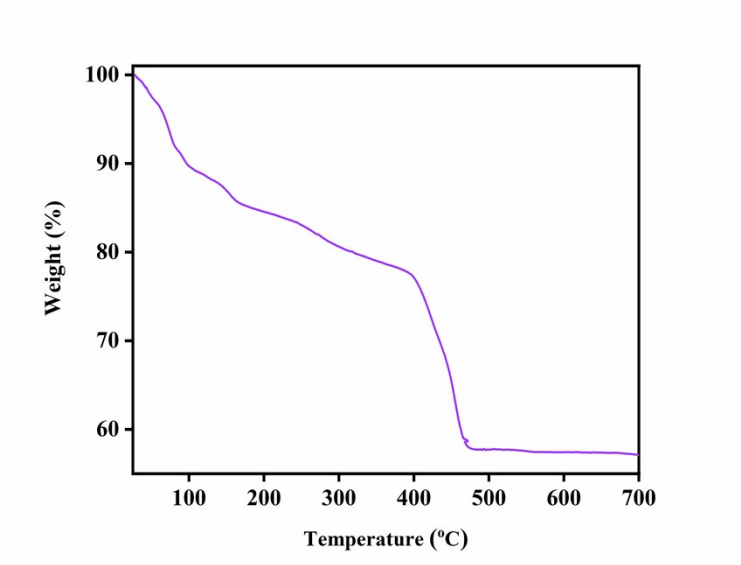

Fig. S22. Thermogravimetric curve of $Se_2As_6Mo_{20}Ce_2$.

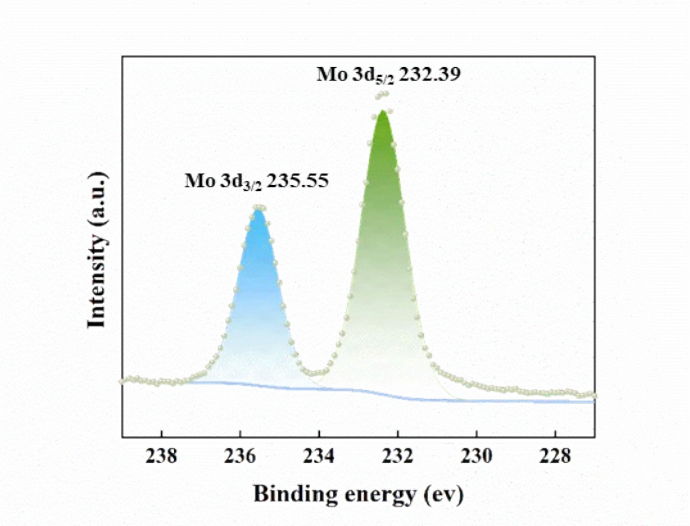

Fig. S23. XPS analysis for Mo^{VI} in $Se_2As_6Mo_{20}Ce_2$.

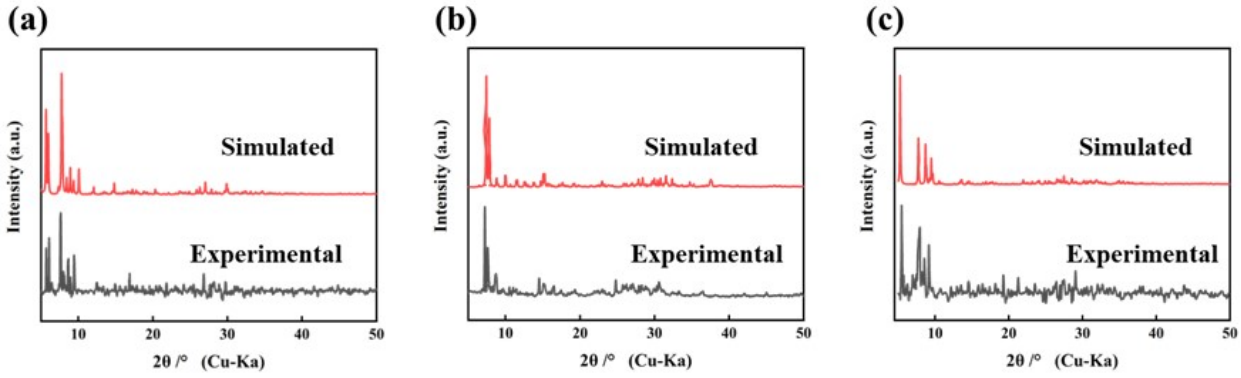

Fig. S24. Powder XRD patterns of $SeAs_3Mo_{10}$ (a), $Se_2As_2Mo_{10}$ (b) and $Se_2As_6Mo_{20}Ce_2$ (c).

Table S1 BVS values for different structural types of addenda and oxygen atoms in **$SeAs_3Mo_{10}$** and **$Se_2As_2Mo_{10}$**

$SeAs_3Mo_{10}$					
Mo	**BVS value**	**O**	**BVS value**	**O**	**BVS value**
Mo1	5.761	O7	1.967	O24	2.198
Mo2	5.966	O8	1.480	O25	1.803
Mo3	5.760	O9	2.570	O26	1.969
Mo4	5.582	O10	2.007	O27	2.362
Mo5	6.104	O11	2.008	O28	1.452
Mo6	5.814	O12	2.165	O29	1.618
Mo7	5.721	O13	1.852	O30	1.533
Mo8	5.724	O14	1.983	O31	2.176
Mo9	5.722	O15	1.618	O32	1.452
Mo10	6.316	O16	1.754	O33	2.317
O	**BVS value**	O17	1.575	O34	1.533
O1	2.243	O18	1.492	O35	1.533
O2	1.865	O19	1.575	O36	1.708
O3	2.044	O20	2.015	O37	2.170
O4	1.741	O21	2.029	O38	1.533
O5	2.438	O22	1.694	O39	2.008
O6	1.708	O23	2.069	O40	2.102
				O41	2.025
$Se_2As_2Mo_{10}$					
Mo	**BVS value**	**O**	**BVS value**	**O**	**BVS value**
Mo12	6.082	O89	1.662	O106	1.618
Mo16	5.867	O90	1.966	O107	1.803
Mo24	5.862	O91	1.708	O108	1.708
Mo25	6.001	O92	1.855	O109	1.533
Mo26	6.230	O93	1.618	O110	1.918
Mo27	5.961	O94	1.618	O111	1.950
Mo28	6.326	O95	2.158	O112	1.662
Mo29	6.013	O96	1.957	O113	1.841
Mo30	6.008	O97	1.921	O114	1.769
Mo31	6.103	O98	1.452	O115	1.662
O	**BVS value**	O99	1.829	O116	2.066
O42	2.022	O100	1.533	O117	1.984
O84	1.983	O101	1.900	O118	1.810
O85	1.662	O102	1.662	O119	1.618
O86	1.846	O103	1.533	O120	2.104
O87	1.575	O104	1.769	O121	1.772
O88	1.929	O105	1.662	O122	1.925
				O123	1.575

Table S2 Assignments and *m*/*z* values for the main peaks observed in the ESI-MS spectra of **$SeAs_3Mo_{10}$** and **$Se_2As_2Mo_{10}$**

$SeAs_3Mo_{10}$	
m*/*z	**Formula**
539.21	$\{(NH_4)_3Mo_4O_{13}(NH_3C_6H_4AsO_3)(SeO_3)(H_2O)_5\}^{2-}$
609.15	$\{(NH_4)_5Mo_6O_{21}(NH_3C_6H_4AsO_3)\}^{2-}$
1272.51	$\{(NH_4)_6Mo_6O_{21}(NH_3C_6H_4AsO_3)(H_2O)_2\}^{-}$
1343.88	$\{(NH_4)_6Mo_6O_{21}(NH_3C_6H_4AsO_3)(H_2O)_6\}^{-}$
$Se_2As_2Mo_{10}$	
m*/*z	**Formula**
475.19	$\{(NH_4)_5Mo_3O_{11}(NH_3C_6H_4AsO_3)(SeO_3)(H_2O)_3\}^{2-}$
539.73	$\{(NH_4)_2Mo_4O_{13}(SeO_3)_2(H_2O)_{11}\}^{2-}$
788.55	$\{(NH_4)_4Mo_3O_{11}(NH_3C_6H_4AsO_3)(H_2O)_2\}^{-}$

Table S3 Condition optimization for the model reaction[a]

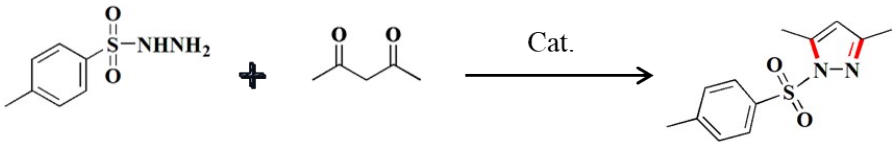

1a **2a** **3a**

Entry	Catalyst (1.5 mol%)	Temp. (°C)	Time (min)	Solvent	Yield[b] (%)
1	—	RT	10	DMC	28
2	—	RT	60	DMC	55
3	$SeAs_3Mo_{10}$	RT	30	DMC	74
4	$SeAs_3Mo_{10}$	RT	60	DMC	93
5	$SeAs_3Mo_{10}$	RT	90	DMC	99
6	$SeAs_3Mo_{10}$	RT	90	DCE	99
7	$SeAs_3Mo_{10}$	RT	90	Ph-Cl	99
8	$Se_2As_2Mo_{10}$	RT	3	DMC	81
9	$Se_2As_2Mo_{10}$	RT	5	DMC	98
10	$Se_2As_2Mo_{10}$	RT	10	DMC	99
11	$Se_2As_2Mo_{10}$	RT	10	DCE	99
12	$Se_2As_2Mo_{10}$	RT	10	Ph-Cl	99
13	$Se_2As_6Mo_{20}Ce_2$	RT	10	DMC	68
14	$Se_2As_6Mo_{20}Ce_2$	RT	30	DMC	97
15	$Se_2As_6Mo_{20}Ce_2$	RT	40	DMC	99
16	$Se_2As_6Mo_{20}Ce_2$	RT	40	DCE	99
17	$Se_2As_6Mo_{20}Ce_2$	RT	40	Ph-Cl	99
18	As_4Mo_{12}	RT	30	DMC	66
19	As_4Mo_{12}	RT	60	DMC	75
20	As_4Mo_{12}	RT	120	DMC	99
21	As_4Mo_{12}	RT	120	DCE	99
22	As_4Mo_{12}	RT	120	Ph-Cl	99

[a] Reaction conditions: *p*-toluenesulfonyl hydrazide **1a** (0.2 mmol), acetylacetone **2a** (0.2 mmol), solvent (0.5 mL). [b] The yields were determined by GC with biphenyl as the internal standard.

Table S4 Dehydration condensation of *p*-toluenesulfonyl hydrazide and acetylacetone by different catalysts[a]

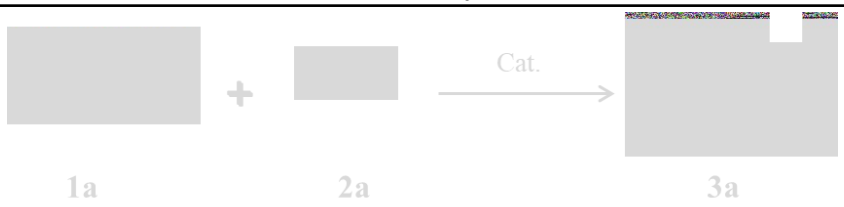

Entry	Catalyst	Temp. (°C)	Time (min)	Solvent	Yield[b] (%)
1	**$SeAs_3Mo_{10}$**	RT	10	DMC	61
2	**$Se_2As_2Mo_{10}$**	RT	10	DMC	99
3	**$Se_2As_6Mo_{20}Ce_2$**	RT	10	DMC	68
4	**As_4Mo_{12}**	RT	10	DMC	56
5	$(NH_4)_6Mo_7O_{24}\cdot 4H_2O$	RT	10	DMC	47
6	*p*-$H_2NC_6H_4AsO_3H_2$	RT	10	DMC	45
7	SeO_2	RT	10	DMC	54
8	Mixture[c]	RT	10	DMC	51
9	—	RT	10	DMC	28

[a] Reaction conditions: *p*-toluenesulfonyl hydrazide **1a** (0.2 mmol), acetylacetone **2a** (0.2 mmol), catalyst (1.5 mol%), and DMC (0.5 mL) at RT for 10 min. [b] Yield was determined by GC with biphenyl as the internal standard. [c] The composition of the mixture is $(NH_4)_6Mo_7O_{24}\cdot 4H_2O$ (1.5 mol%), *p*-$H_2NC_6H_4AsO_3H_2$ (1.5 mol%) and SeO_2 (1.5 mol%).

Table S5 Comparison of the catalytic efficiency of POM-based catalysts in the condensation-cyclization reactions of *p*-toluenesulfonyl hydrazide and acetylacetone

Catalyst	Conditions	Catalyst Loading (mmol)	Yield (%)
$[NaCo_2Mo_2O_7(OH)_3]_n$[S8]	80 °C, 60 min	2×10^{-2}	98
$[Cu_3(\mu_3\text{-}OH)(tba)_3(Htba)(H_2O)_2(HPMo_{12}O_{40})]\cdot7H_2O$[S9] (Htba = 3-(4H-1,2,4-triazol-4-yl)-benzoic acid)	80 °C, 90 min	1×10^{-2}	99
$(NH_4)_7[(SeO_3)_2Mo_{12}O_{36}(CH_3COO)_3]14H_2O$[S10]	RT, 60 min	3×10^{-3}	99
$(NH_4)_4[(SeO_3)_{1.3}(HPO_3)_{0.7}Mo_{12}O_{36}(NH_3CH_2COO)_3]10H_2O$[S10]	RT, 60 min	3×10^{-3}	99
$(NH_4)_4[(SeO_3)_{1.4}(HPO_3)_{0.6}Mo_{12}O_{36}(L\text{-}NH_3C_2H_3OHCOO)_3]18H_2O$[S10]	RT, 60 min	3×10^{-3}	99
$Na_3[H_{19}(UO_2)_2O(Se_2W_{14}O_{52})_2]\cdot41H_2O$ [S11]	80 °C, 60 min	2×10^{-3}	98
$(C_2H_8N)_{12}Na_2[H_{10}\{Ce(H_2O)_5\}_2(Te_2W_{37}O_{132})]\cdot39H_2O$ [S12]	80 °C, 60 min	1×10^{-3}	99
$Na_{11}H(H_2O)_{31}[Na(UO_2)(A\text{-}PW_9O_{34})]_2\cdot7H_2O$ [S13]	80 °C, 60 min	1×10^{-2}	99
$SeAs_3Mo_{10}$ (This Work)	RT, 90 min	3×10^{-3}	99
$Se_2As_2Mo_{10}$ (This Work)	RT, 10 min	3×10^{-3}	99
$Se_2As_6Mo_{20}Ce_2$ (This Work)	RT, 40 min	3×10^{-3}	99

Table S6 Acetalization of 2-aminobenzamide and benzaldehyde by different catalysts[a]

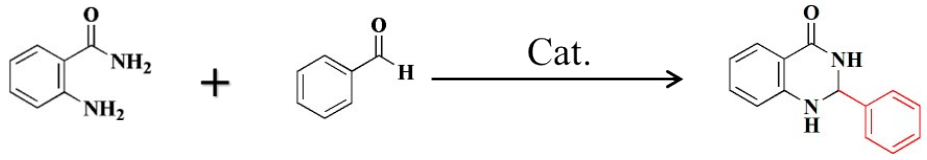

Entry	Catalyst	Conditions	Catalyst Loading (mmol)	Solvent	Yield[b] (%)
1	—	80 °C, 2 h	—	CH_3CN	13
2	**$SeAs_3Mo_{10}$**	80 °C, 2 h	3×10^{-3}	CH_3CN	99
3	**$Se_2As_2Mo_{10}$**	80 °C, 1 h	3×10^{-3}	CH_3CN	99
4	**$Se_2As_6Mo_{20}Ce_2$**	80 °C, 2 h	3×10^{-3}	CH_3CN	99
5	**As_4Mo_{12}**	80 °C, 2 h	3×10^{-3}	CH_3CN	89
6	**SRMIST−1**[S14]	Reflux, 10 h	2.5×10^{-3}	EtOH	99
7	**$Na_{3.3}H_{2.7}(H_2O)_9[Ni_{0.58}UMo_{12}O_{42}]\cdot4.5H_2O$**[S15]	80 °C, 9 h	6×10^{-3}	CH_3CN	91

[a] Reaction conditions: 2-aminobenzamide (0.2 mmol), benzaldehyde (0.2 mmol), catalyst (1.5 mol%), and acetonitrile (1.0 mL) at 80 °C and different reaction time. [b] Yield was determined by GC with biphenyl as the internal standard.

Table S7 Crystal data and structure refinement for the as-made compounds

Compound	**$SeAs_3Mo_{10}$**	**$Se_2As_2Mo_{10}$**	**$Se_2As_6Mo_{20}Ce_2$**
Empirical formula	$SeAs_3Mo_{10}C_{18}H_{63}N_6O_{56}$	$Se_2As_2Mo_{10}C_{12}H_{52}N_6O_{52}$	$Ce_2Se_2As_6Mo_{20}C_{36}H_{136}N_6O_{129}$
Formula weight, g/mol	2522.82	2379.71	5523.91
Crystal system	Orthorhombic	Triclinic	Triclinic
Space group	*Pbcn*	*P*-1	*P*-1
a, Å	31.326(3)	13.930(3)	12.1018(14)
b, Å	23.4652(19)	20.189(5)	15.6636(19)
c, Å	24.275(2)	24.369(6)	22.209(3)
α, °	90	91.991(7)	99.665(4)
β, °	90	99.609(8)	94.683(4)
γ, °	90	90.075(8)	108.620(4)
Volume, Å^3	17844(3)	6753(3)	3891.5(8)
Z	8	2	1
D_{calc}, g/cm^3	1.637	2.021	2.076
Absorption coefficient, mm^{-1}	2.931	3.550	3.941
F(000)	8248	3833	2270
Theta range for data collection, °	2.12 to 25.00	2.16 to 25.00	2.40 to 28.38
Completeness to Θ_{max}	99.9 %	98.1 %	99.9 %
Index ranges	-37<=h<=36 -27<=k<=27 -27<=l<=28	-16<=h<=16 -23<=k<=24 -28<=l<=28	-16<=h<=16 -20<=k<=20 -29<=l<=29
Reflections collected	136137	77446	87718
Independent reflections	15705	23326	19408
R(int)	0.2492	0.0569	0.0579
Absorption correction	Semi-empirical from equivalents	Semi-empirical from equivalents	Semi-empirical from equivalents
Data / restraints / parameters	15705 / 270 / 688	23326 / 4298 / 1259	19408 / 36 / 778
Goodness-of-fit on F^2	1.078	1.226	1.049
R_1,[a] wR_2[b] ($I > 2\sigma(I)$)	R_1 = 0.0619 wR_2 = 0.1647	R_1 = 0.1410 wR_2 = 0.3559	R_1 = 0.0309 wR_2 = 0.0724
R_1,[a] wR_2[b] (all data)	R_1 = 0.0759 wR_2 = 0.1721	R_1 = 0.1878 wR_2 = 0.3731	R_1 = 0.0422 wR_2 = 0.0759
Largest diff. peak and hole, e/Å^3	1.875 and -1.870	7.396 and -3.177	1.983 and -1.223

[a] $R_1 = \Sigma||F_o| - |F_c||/\Sigma|F_o|$. [b] $wR_2 = [\Sigma w(F_o^2 - F_c^2)^2/\Sigma w(F_o^2)^2]^{1/2}$.

References

S1 G. M. Sheldrick, *Acta Cryst.*, 2015, **C71**, 3–8.
S2 G. M. Sheldrick, *Acta Cryst.*, 2008, **A64**, 112–122.
S3 O. V. Dolomanov, L. J. Bourhis, R. J. Gildea, J. A. K. Howard and H. Puschmann, *J. Appl. Cryst.*, 2009, **42**, 339–341.
S4 A. L. Spek, *Acta Cryst.*, 2015, **C71**, 9–18.
S5 M. J. Frisch, G. W. Trucks, H. B. Schlegel, G. E. Scuseria, M. A. Robb, J. R. Cheeseman, G. Scalmani, V. Barone, B. Mennucci, G. A. Petersson, H. Nakatsuji, M. Caricato, X. Li, H. P. Hratchian, A. F. Izmaylov, J. Bloino, G. Zheng, J. Hasegawa, M. Ishida, T. Nakajima, Y. Honda, O. Kitao, H. Nakai, T. Vreven, J. A. M ontgomery Jr, J. E. Peralta, F. Ogliaro, M. Bearpark, J. J. Heyd, E. Brothers, K. N. Kudin, V. N. Staroverov, R. Kobayashi, J. Normand, K. Raghavachari, A. Rendell, J. C. Burant, S. S. Iyengar, J. Tomasi, M. Cossi, N. Rega, J. M. Millam, M. Klene, J. E. Knox, J. B. Cross, V. Bakken, C. Adamo, J. Jaramillo, R. Gomperts, R. E. Stratmann, O. Yazyev, A. J. Austin, R. Cammi, C. Pomelli, J. W. Ochterski, R. L. Martin, K. Morokuma, V. G. Zakrzewski, G. A. Voth, P. Salvador, J. J. Dannenberg, S. Dapprich, A. D. Daniels, O. Farkas, J. B. Foresman, J. V. Ortiz, J. Cioslowski and D. J. Fox, Gaussian09W, Revision A02, Gaussian, Inc., Wallingford, CT, 2009.
S6 (a) A. D. Becke, *J. Chem. Phys.*, 1993, **98**, 5648; (b) C. Lee, W. Yang and R. G. Parr, *Phys. Rev. B: Condens. Matter Mater. Phys.*, 1988, **37**, 785.
S7 J. Tomasi, B. Mennucci and R. Cammi, *Chem. Rev.*, 2005, **105**, 2999–3094.
S8 G. Yang, Y. Liu, X. Lin, B. Ming, K. Li and C.Hu, *Chin. Chem. Lett.*, 2022, **33**, 354–357.
S9 K. Li, Y.-F. Liu, X.-L. Lin and G.-P. Yang, *Inorg. Chem.*, 2022, **61**, 6934–6942.
S10 L.-L. Liu, Y.-H. Wang, X.-Y. Xiao, K.-W. Tong, Y. Zhao, C.-Q. Chen, J. Du and P. Yang, *Rare Met.*, 2023, **42**, 3345–3353.
S11 M. Cheng, Y. Liu, W. Du, J. Shi, J. Li, H. Wang, K. Li, G. Yang and D. Zhang, *Chin. Chem. Lett*., 2022, **33**, 3899–3902.
S12 G.-P. Yang, S.-X. Shang, B. Yu and C.-W. Hu, *Inorg. Chem. Front*., 2018, **5**, 2472–2477.
S13 G.-P. Yang, X.-L. Zhang, Y.-F. Liu, D.-D. Zhang, K. Li and C.-W. Hu, *Inorg. Chem. Front*., 2021, **8**, 4650–4656.
S14 V. Jeevananthan, G. C. Senadi, K. Muthu, A. Arumugam and S. Shanmugan, *Inorg. Chem.,* 2024, **63**, 5446–5463.
S15 K. Li, Y. F. Liu, G. P. Yang, Z. J. Zheng, X. L. Lin, Z. B. Zhang, S. J. Li, Y. H. Liu and Y. G. Wei, *Green Chem.,* 2024, **26**, 6454–6460.